Journal of Geophysical Research: Atmospheres

RESEARCH ARTICLE
10.1029/2018JD028300

Key Points:
- Mixing fraction of tropospheric/stratospheric air masses in the tropical 400 K during 1980–2016 was evaluated using trajectory analysis
- The stratospheric mixing fraction shows positive (negative) trends before (after) 1999; their impact on stratospheric age of air is examined
- The separate contributions of several processes to the age of air in the midlatitude middle stratosphere are estimated

Correspondence to:
Y. Inai,
yoichi_inai@tohoku.ac.jp

Citation:
Inai, Y. (2018). Long-term variation in the mixing fraction of tropospheric and stratospheric air masses in the upper tropical tropopause layer. *Journal of Geophysical Research: Atmospheres*, *123*, 4890–4909. https://doi.org/10.1029/2018JD028300

Received 9 JAN 2018
Accepted 19 APR 2018
Accepted article online 30 APR 2018
Published online 17 MAY 2018

Long-Term Variation in the Mixing Fraction of Tropospheric and Stratospheric Air Masses in the Upper Tropical Tropopause Layer

Yoichi Inai[1]

[1]Center for Atmospheric and Oceanic Studies, Graduate School of Science, Tohoku University, Sendai, Japan

Abstract Observational records of the stratospheric mean age of air (AoA), the average transit time of an air parcel since entering the stratosphere, must reflect changes in the in-mixing from the extratropical lower stratosphere to the tropical tropopause layer (TTL). Focusing on the mixing fraction of tropospheric and stratospheric air masses in the upper TTL, the impact of mixing processes that occur prior to air masses entering the stratosphere separately from those that occur within the stratosphere is investigated. Using trajectory analysis, the mixing fraction during 1980–2016 is evaluated, and AoA and water vapor mixing ratios in the upper TTL are reconstructed. The interannual variation in the reconstructed water vapor shows good agreement with observations in the tropics. Furthermore, the reconstructed AoA exhibits long-term variation with a positive trend between 1980 and 1999. To compare the reconstructed AoA with the observed AoA in the midlatitude stratosphere, the transit time spectra are estimated for the 1989–2016 period, and the AoA in the midlatitude stratosphere is estimated by integration of the spectrum together with the AoA in the upper TTL. As a result, although the explicitly calculated transit time shows a clear underestimation compared with previous studies, it is suggested that the "aging" effects are 3.1–4.2 years for transit time in the stratosphere, 0.2–0.7 years for in-mixing prior to entering the stratosphere, 0.1 years for transit time from the troposphere to upper TTL, and 0.0–1.6 years for subgrid-scale mixing in the stratosphere.

1. Introduction

The stratospheric meridional transport, the Brewer-Dobson circulation (BDC), which consists of shallow and deep branches, largely controls the temporal-spatial distribution of the chemical composition of the lower stratosphere (LS). The BDC strength and its variation are often quantified using the mean age of air (AoA), the average transit time of an air parcel since entering the stratosphere (Hall & Plumb, 1994; Kida, 1983). The AoA is typically estimated from the relative concentration of a "clock tracer" (e.g., Hall & Plumb, 1994) at any point in the stratosphere compared with that in the troposphere. Many numerical models have predicted that increasing concentrations of greenhouse gases are intensifying the BDC, including both its shallow and deep branches (e.g., Butchart et al., 2010; Li et al., 2012; Waugh et al., 2009) and that AoA should therefore decrease over time. However, observational AoA estimates show no such negative trend in the Northern Hemisphere (NH; Engel et al., 2009, 2017; Haenel et al., 2015). Addressing this discrepancy, Garny et al. (2014), Ploeger et al. (2015), and Dietmüller et al. (2017) suggested that the mixing process in the stratosphere plays a crucial role in determining trends in AoA.

Stratospheric mixing leads to a net aging of stratospheric air masses, via the mixing of high-latitude older air masses into the tropical stratosphere, in turn causing recirculation. Meridional mixing such as this is largely a result of planetary-scale Rossby wave breaking (this process also drives the deep branch of the BDC). In particular, mixing between the tropical tropopause layer (TTL) and the extratropical LS also occurs. For example, Rossby wave breaking at the subtropical tropopause in the vicinity of the subtropical jet stream can transport stratospheric air into the tropical upper and middle troposphere (e.g., Gettelman et al., 2011; Manney et al., 2011) as well as into the TTL. In addition, stratospheric tracers are carried to the TTL by anticyclonic circulation associated with the Asian monsoon in boreal summer (e.g., Ploeger et al., 2012; Randel & Jensen, 2013; Santee et al., 2017), yet the monsoon also supplies lower tropospheric air to the upper troposphere (UT) and LS (e.g., Konopka et al., 2010; Orbe et al., 2015; Pan et al., 2016; Ploeger et al., 2017; Vogel et al., 2016). Generally, over the course of a full year, tropical convection uplifts tropospheric air into the TTL and the uplifted tropospheric air masses mix there with the in-mixed stratospheric air masses that come from the extratropical LS. According to estimates from aircraft campaigns in the UT/LS over the tropics, isentropic transport from the

extratropical LS was found to account for 20–40% of the whole air mass around the 400-K potential temperature level over the tropics by Sargent et al. (2014), while it was previously estimated to be only a small percentage by Volk et al. (1996). The mixing fraction of in-mixed stratospheric air masses can vary according to location and time, and the mixed air mass in the TTL is further transported into the tropical LS (TLS) and deeper stratosphere, driven by the BDC.

Though Ploeger et al. (2015) and Dietmüller et al. (2017) included the mixing process between the TTL and extratropical LS in their analyses; their studies did not separate the contributions of mixing into the TTL and of mixing in the stratosphere. In contrast, by focusing on AoA in the upper TTL, this study attempts to quantify the contribution of mixing processes that occur before air masses enter the stratosphere separately from processes that occur within the stratosphere. In other words, the focus of this work is on the mixing process between the TTL and extratropical LS, in particular on the mixing fraction of tropospheric and stratospheric air masses in the upper TTL and how its long-term variation contributes to changes in stratospheric AoA. To compare the estimates of AoA reconstructed from the mixing fraction in the upper TTL with estimates of AoA based on observations of the deep stratosphere (Engel et al., 2009, 2017), the transit time from the upper TTL to the deep stratosphere is also considered. Finally, the effects of the mixing process prior to entering the stratosphere on AoA variation observed in the deep stratosphere are quantified. By reconstructing AoA together with water vapor once on the tropical 400-K surface, (1) prior knowledge of mixing fraction and AoA variations on the 400-K surface is acquired, (2) they are verified from comparison with available observational results in the TLS, and (3) the contributions on the "aging" effect from the deeper stratospheric processes and those prior to entering the stratosphere are examined separately.

2. Methods

2.1. Estimation of Mixing Fraction in the Upper TTL

To identify the origin of air masses in the upper TTL, kinematic backward trajectories were calculated for 90 days following the method of Hasebe and Noguchi (2016). Backward trajectories were initialized at uniformly distributed grid points (every 5.0° longitude by 1.5° latitude) within 20°N and 20°S at the 400-K potential temperature surface. The initializations are made at 00Z on the 5th, 15th, and 25th of every month from January 1980 to December 2016, with meteorological conditions prescribed by the European Centre For Medium-Range Weather Forecasts (ECMWF) ERA-Interim data set (1.5° × 1.5° horizontal, 6-hourly temporal resolutions, with 37 vertical levels; Dee et al., 2011).

For each run, trajectories were categorized as either tropospheric (trj_T) or stratospheric trajectories (trj_S). Trajectories were categorized as trj_T if the trajectory passed through a region below the 350-K potential temperature level and equatorward of 30°N and 30°S for at least 5 days (this criterion is denoted as cri_T). Trajectories were categorized as trj_S if the trajectory passed through regions above 4 potential vorticity unit (PVU) potential vorticity and poleward of 30°N and 30°S for at least 5 days (this criterion is denoted as cri_S). All trajectories were categorized as either trj_T or trj_S, whichever was satisfied first within 90 days of the calculation, or the rest which did not satisfy both cri_T and cri_S within 90 days. Each trj_T was considered to be associated with an air parcel once it reached 400 K after passing along its trajectory from the troposphere. The same applies to stratospheric air parcels, which are represented by trj_S. The mixing fractions of tropospheric and stratospheric air parcels (denoted as f_T and f_S, respectively) were estimated for each set of trajectories. Denoting the number of trj_T and trj_S as N_T and N_S for each run, the mixing fractions were calculated as

$$f_T = \frac{\sum_{i=1}^{N_T} \cos\varnothing_{\mathrm{trj}_T\mathrm{ini}}(i)}{\left(\sum_{i=1}^{N_T} \cos\varnothing_{\mathrm{trj}_T\mathrm{ini}}(i) + \sum_{i=1}^{N_S} \cos\varnothing_{\mathrm{trj}_S\mathrm{ini}}(i)\right)} \text{ and} \tag{1}$$

$$f_S = \frac{\sum_{i=1}^{N_S} \cos\varnothing_{\mathrm{trj}_S\mathrm{ini}}(i)}{\left(\sum_{i=1}^{N_T} \cos\varnothing_{\mathrm{trj}_T\mathrm{ini}}(i) + \sum_{i=1}^{N_S} \cos\varnothing_{\mathrm{trj}_S\mathrm{ini}}(i)\right)}, \tag{2}$$

where $\varnothing_{\mathrm{trj}_T\mathrm{ini}}$ and $\varnothing_{\mathrm{trj}_S\mathrm{ini}}$ indicate the initial latitude of individual backward trajectories initialized within the 20°N to 20°S zonal band. Only trajectories that satisfied either cri_T or cri_S were used (i.e., $f_T + f_s = 1$). Though some trajectories were categorized as either trj_T or trj_S, these amount to less than 15% of the total number. It was confirmed that the results did not qualitatively change using this simplification (see section 3.1).

Table 1
Assumed Water Vapor Mixing Ratio and AoA in the Extratropical Lower Stratosphere (X_{LS} [ppmv] and Γ_{LS} [year]; see section 2.2 for details)

Variable	January	February	March	April	May	June	July	August	September	October	November	December
X_{LS} (NH)	4.0	4.0	4.0	4.0	4.0	4.5	5.0	5.0	5.5	5.5	5.0	4.5
X_{LS} (SH)	4.0	4.0	4.0	4.0	4.0	4.0	4.5	4.5	4.5	4.5	4.5	4.0
Γ_{LS} (NH)	2.0	2.5	3.0	3.0	2.5	2.0	1.5	1.5	1.0	1.0	1.5	2.0
Γ_{LS} (SH)	1.5	1.5	1.5	1.5	1.5	2.0	2.0	2.5	3.0	3.0	2.5	2.0

Note. Values are assumed by reference to Randel and Jensen (2013) and Bönisch et al. (2009) for X_{LS} and Γ_{LS}, respectively. AoA = age of air; NH = Northern Hemisphere; SH = Southern Hemisphere.

The above method for the estimation of the mixing fraction is similar to the approach of Ploeger et al. (2012), except for the following differences. First, the conditions for the trajectory calculations were 3-month kinematic trajectories initialized within 20°N–20°S in the current study compared with 5-month diabatic trajectories initialized within 30°N–30°S in Ploeger et al. (2012). Second, the definition to classify tropospheric or stratospheric trajectories used here was a combination of latitude and potential vorticity, whereas Ploeger et al. (2012) used equivalent latitude. However, according to Ploeger et al. (2012), such differences in these points have no significant impact on the conclusions. To confirm this, we tested the results obtained from the method detailed in this section to the sensitivity of different boundary values or equivalent latitude instead of latitude. The results show that the estimated mixing fractions are qualitatively robust to such changes; in particular, their interannual variation pattern is essentially independent from such choices (see Appendix A).

2.2. Reconstruction of Water Vapor and AoA in the Upper TTL

A change in the ratio of f_T to f_S should affect the relative abundance of chemical species in the TLS, as well as water vapor and AoA. In particular, its long-term variation should influence water vapor and AoA trends in the TLS. For example, Ploeger et al. (2012) reconstructed water vapor, carbon monoxide, and ozone mixing ratios in the tropical UT/LS using estimated tropospheric and stratospheric mixing fractions. Following their study, mixing fraction estimates were used to reconstruct water vapor mixing ratio and AoA in the upper TTL. Conceptually, the time series of water vapor (X^{t400}) and AoA (Γ^{t400}) at the 400-K potential temperature in the upper TTL were reconstructed from the time series of the mixing fractions and the assumed water vapor mixing ratios (X_T/X_S) and AoAs (Γ_T/Γ_S) for tropospheric/stratospheric air masses, respectively, as

$$X^{t400} = f_T * X_T + f_S * X_S \text{ and} \tag{3}$$

$$\Gamma^{t400} = f_T * \Gamma_T + f_S * \Gamma_S. \tag{4}$$

The tropospheric mixing ratio, X_T, is calculated from the Lagrangian minimum saturation water vapor mixing ratio (SMR_{min}) and saturation ratio (α), while Γ_T is calculated from the time to satisfy the cri_T along trj_T (τ_T), respectively, as

$$X_T = \frac{\sum_{i=1}^{N_T} \alpha * SMR_{min}(i) * \cos\varnothing_{trj_T ini}(i)}{\sum_{i=1}^{N_T} \cos\varnothing_{trj_T ini}(i)} \text{ and} \tag{5}$$

$$\Gamma_T = \frac{\sum_{i=1}^{N_T} \tau_T(i) * \cos\varnothing_{trj_T ini}(i)}{\sum_{i=1}^{N_T} \cos\varnothing_{trj_T ini}(i)}. \tag{6}$$

Table 2
Assumed Supersaturation Ratio Assigned to α in Equation (5)

Temperature (K)	< 185.0	[185.0, 187.5)	[187.5, 190.0)	≥190.0
Saturation ratio α	1.3	1.2	1.1	1.0

Note. Values are assumed by reference to Krämer et al. (2009).

Here α is assigned a value from 1.0 to 1.3 depending on temperature (Table 1), which is obtained from Figures 4 and 7 of Krämer et al. (2009). On the other hand, the stratospheric mixing ratio, X_S, is considered to be a seasonally varying mixing ratio (Table 2), while Γ_S is determined as $\Gamma_S = \Gamma_{adv} + \Gamma_{LS}$, where Γ_{adv} is calculated from the time to satisfy cri_S along trj_S (τ_S) and Γ_{LS} is also considered to be seasonally varying (Table 2), respectively, as

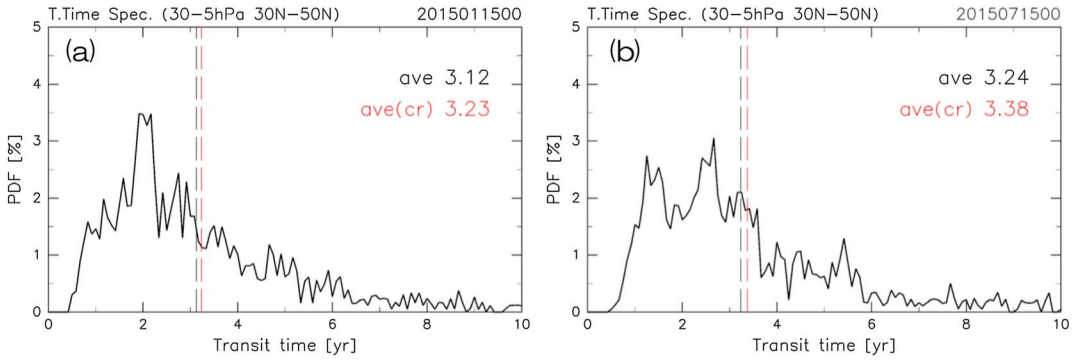

Figure 1. Examples of the transit time spectrum in the midlatitude middle stratosphere in the altitude/latitude region of 30–5 hPa/30°N–50°N (corresponding to the observational region of Engel et al. (2009, 2017)) calculated for 00Z 15th (a) January and (b) July 2015. The black vertical dashed lines show mean transit time for the spectrum, while the red vertical dashed lines show that for the tail-corrected spectrum using an exponential fit (see text in section 2.3).

$$X_S = \frac{\sum_{i=1}^{N_S} X_{LS}(t-\tau_S(i))*\cos\varnothing_{trj_S ini}(i)}{\sum_{i=1}^{N_S} \cos\varnothing_{trj_S ini}(i)}, \tag{7}$$

$$\Gamma_S = \frac{\sum_{i=1}^{N_S} \tau_S(i)*\cos\varnothing_{trj_S ini}(i)}{\sum_{i=1}^{N_S} \cos\varnothing_{trj_S ini}(i)} + \frac{\sum_{i=1}^{N_S} \Gamma_{LS}(t-\tau_S(i))*\cos\varnothing_{trj_S ini}(i)}{\sum_{i=1}^{N_S} \cos\varnothing_{trj_S ini}(i)}, \tag{8}$$

where t in equations (7) and (8) is the time when trajectories were launched for each run. The seasonally varying X_{LS} and Γ_{LS} simulate a seasonal cycle of water vapor and AoA in the extratropical LS, especially in association with the Asian Monsoon (e.g., Ploeger et al., 2013; Randel & Jensen, 2013); hence, they are assigned hemispherically dissymmetric values according to which hemisphere the individual trj_S originated. The values assigned to X_{LS} and Γ_{LS} were obtained from Figure 2 of Randel and Jensen (2013) and Figure 2 of Bönisch et al. (2009), respectively. The water vapor reconstruction X^{t400} was compared with observational estimates in the TLS from both satellite and balloon.

2.3. Treatment of Transport in the Stratosphere

When comparing the reconstruction to observations of the midlatitude middle stratosphere—such as the AoA estimates by Engel et al. (2009, 2017)—the transit time, which has a broad spectrum (e.g., Waugh & Hall, 2002), should be taken into account, because the reconstruction is estimated for only the upper TTL. Therefore, the transit time (τ) was estimated from backward trajectories, starting in the midlatitude region consistent with that of Engel et al. (2009, 2017) and tracing back to 400 K within 20°N and 20°S for a period of 10 years. The initial points were zonally set at grid points (i.e., every 5.0° longitude by 5.0° latitude) within 30°N and 50°N on 30-, 19-, 12-, 8-, and 5-hPa pressure surfaces. A total of 1,800 trajectories for each run was launched at 00Z on the 15th day of every month from January 1989 to December 2016. The results from this calculation were used to construct the transit time spectra. For example, the probability distribution functions (PDFs) are defined as a function of the transit time, τ, and trajectory launching time, t ($\equiv p(t,\tau)$). Thus, the mean transit time, T, is estimated by

$$T(t) = \int_0^{\tau_{fin}} \tau * p(t,\tau) d\tau, \tag{9}$$

where τ_{fin} is equal to 10 years in this study. Figure 1 presents two examples of the estimated transit time spectrum calculated, starting at 00Z on 15 January and 15 July in 2015. The PDF interval is 1 month with the area-weighted function according to the initial latitude of individual backward trajectories. The mean transit times in these examples are estimated to be 3.12 and 3.24 years for January and July of 2015, respectively.

According to Diallo et al. (2012) and Ploeger and Birner (2016), T obtained by equation (9) underestimates actual mean transit time to some degree, due to the truncated integration up to τ_{fin} = 10 years. Therefore, we similarly apply a correction for the finite spectrum tail using an exponential fit (Diallo et al., 2012; Ploeger & Birner, 2016) to estimates of mean transit time. To apply the correction, a modified version of equation (9) is expressed as

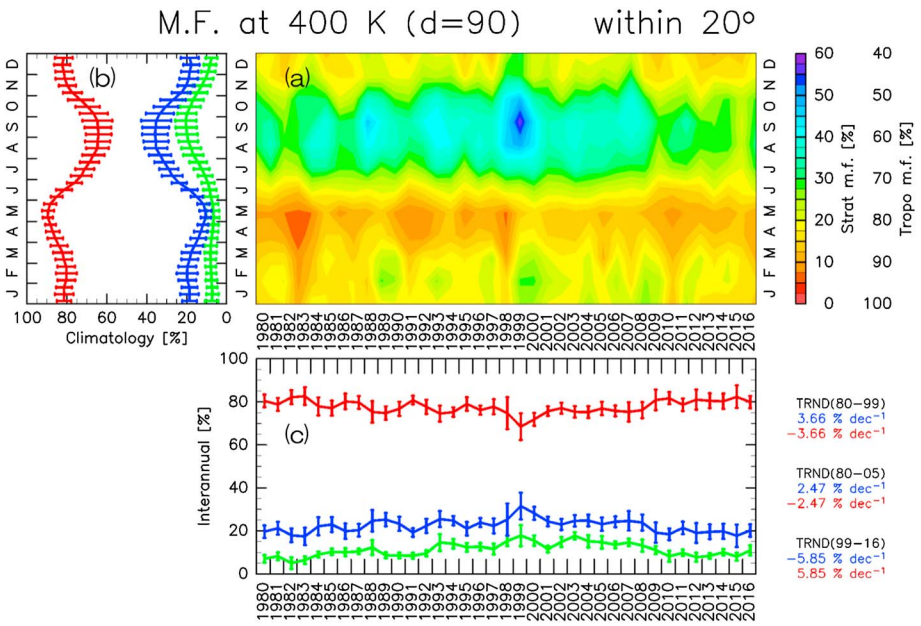

Figure 2. (a) Monthly averaged mixing fraction at the 400-K potential temperature surface, averaged over 20°S–20°N, shown as a year-month cross section; (b) the seasonal variation of tropospheric (red) and stratospheric (blue) mixing fractions, and (c) the interannual variation of tropospheric (red) and stratospheric (blue) mixing fractions. The bars indicate one standard deviation. For (a) and (b), the mixing fractions of noncategorized trajectories are also shown in green for comparison.

$$T(t) = \int_0^{\tau_{\text{fin}}} \tau * p(t,\tau) \mathrm{d}\tau + p(t,\tau_{\text{fin}}) * \left(\tau_{\text{fin}} + \frac{1}{b}\right) \tag{10}$$

where b is the exponential decrement factor (see also Diallo et al., 2012, their equation 2) calculated for an individual spectrum by fitting the exponential function for transit times 5 years $< \tau <$ 10 years following Ploeger and Birner (2016) after changing the PDF interval to 1 year. The contribution of this correction is also shown in Figure 1. The mean transit times after this correction are 3.23 and 3.38 years for January and July of 2015, respectively. The tail correction is rather weak, especially when compared with Ploeger and Birner (2016), presumably due to limiting the analytical region up to 1 hPa, the highest pressure level of the data set used. Herein, we use the tail-corrected mean transit time in the remainder of the study. Lastly, AoA in the midlatitude stratosphere ($\Gamma^{\text{mid-st}}$) is reconstructed from the sum of the mean transit time, T, and the integration of AoA at the 400 K Γ^{t400} with the PDF, represented as

$$\Gamma^{\text{mid-st}}(t) = T(t) + \int_0^{\tau_{\text{fin}}} \Gamma^{t400}(t-\tau) * p(t,\tau) \mathrm{d}\tau. \tag{11}$$

Preferably, the second term on the right-hand side of equation (11) is to be integrated from zero to infinity. However, the integration can be truncated with no significant effect on the results because p approaches zero (typically less than 4% even if p is integrated from 10 years to infinity) and Γ^{t400} is small (typically ~0.5 years as shown in section 3.2).

3. Results

3.1. Mixing Fraction

The mixing fraction was calculated three times every month between 1980 and 2016 and then monthly averaged. A year-month cross section of averaged mixing fraction is shown in Figure 2a. The stratospheric mixing fraction has a strong seasonal variation, with high values during August–October and low values during April–May. This pattern is reversed for the tropospheric mixing fraction. Annual means of stratospheric mixing fraction increased between 1980 and 1999 but decreased between 1999 and 2016. The reverse is true for the tropospheric mixing fraction. The largest interannual variations appear in September.

To quantify the seasonal variation in the mixing fractions, averaged f_T and f_S are shown as a 37-year climatology (Figure 2b). f_T ranges from ~60% to ~90% with a maximum value in May, while f_S ranges from

~10% to ~40% with a maximum in September. The seasonal enhancement of f_S during the boreal summer is likely the result of Asian monsoon activity. Comparing the seasonal variations here with those of Ploeger et al. (2012), it was found that f_S is qualitatively similar but approximately twice as large as their estimate through a whole year. Nonetheless, the discrepancy between the two is within the range of uncertainty for mixing fraction estimates (see Appendix A). The results described here are also consistent with studies based on aircraft measurement campaigns in the same region. For example, Homan et al. (2010) estimated the mixing fraction of a stratospheric air mass at 390-K potential temperature over central Africa as ~30% in August 2006, while the estimate in this work is ~40% for the same spatiotemporal region (15°W–10°E, 20°N–0°N) in early August 2006. Sargent et al. (2014) estimated the mixing fraction of a stratospheric air mass at 400-K potential temperature over Central America as ~30% during January–February 2006 and in August 2007, while estimates presented here are 5–25% and 15–40% for this region (100°W–70°W, 20°N–10°S) in January–February 2006 and in August 2007, respectively. On the other hand, the conservative estimate by Ploeger et al. (2012) is in good agreement with Volk et al. (1996), and this point is discussed in Appendix B.

Annual averages of f_T and f_S ($\equiv\overline{f_T}$ and $\overline{f_S}$) are calculated after their deseasonalization for 1980 to 2016 (Figure 2c). $\overline{f_T}$ was ~80% in 1980 but fell to ~70% in 1999, while $\overline{f_S}$ was ~20% in 1980 but rose to ~30% in 1999. The long-term variations between 1980 and 1999 result in negative (-3.7%/decade) and positive (3.7%/decade) trends for $\overline{f_T}$ and $\overline{f_S}$, respectively. In contrast, between 1999 and 2016 the trend is reversed, with values of 5.9%/decade for $\overline{f_T}$ and -5.9%/decade for $\overline{f_S}$. According to sensitivity analyses (Appendix A), although the annual averages of mixing fractions are strongly dependent on the choice of the stratospheric origin criterion, the variability is robust. If these estimated interannual variations are accurate, they should also be reflected in observational records, and the corresponding changes in the water vapor mixing ratio and AoA in the upper TTL and TLS should be verified.

Note here that the mixing fraction of noncategorized trajectories ($\equiv f_R$) is also plotted for comparison in Figures 2b and 2c. It is evident that the variation pattern in f_R is similar to that in f_S. This suggests that seasonal and interannual variations in AoA reconstructed in the upper TTL do not qualitatively change if f_R is included in the reconstruction under the assumption that the noncategorized trajectories have some AoA, whereby the value is larger than Γ_T and smaller than Γ_S.

3.2. Water Vapor and AoA in the Upper TTL

The water vapor mixing ratio, X^{t400}, and AoA Γ^{t400} were reconstructed using equations (3) and (4), respectively. Their monthly averaged values are shown in Figure 3 and range from approximately 2.5 to 5.8 ppmv for X^{t400} and from approximately 0.2 to 1.0 years for Γ^{t400}. The averaged advection time back to the troposphere, Γ_T, estimated by equation (6) is also shown in Figure 3b for comparison. The difference between Γ^{t400} and Γ_T can be considered as the contribution of air mass mixing from the extratropical LS to TTL. While both X^{t400} and Γ^{t400} exhibit obvious seasonal variations with peak-to-peak amplitude of typically 2 ppmv for X^{t400} and 0.4 years for Γ^{t400}, they also have interannual variations.

To clarify the interannual, as well as seasonal, variations in the series, their seasonal variations are quantified by their 37-year climatology, whereas their annual averages ($\equiv\overline{X^{t400}}$ and $\overline{\Gamma^{t400}}$) are obtained after deseasonalization. Figure 4 shows the interannual and seasonal variations for X^{t400} together with the water vapor mixing ratio at 83 hPa measured by the Microwave Limb Sounder (MLS) onboard the Aura satellite. The MLS data were zonally averaged within 20°N and 20°S. The annual averaged water vapor reconstruction $\overline{X^{t400}}$ varies over time similar to the MLS measurements but with smaller amplitude. Over the period from 1980 to 1999, $\overline{X^{t400}}$ has a positive trend of 0.14 ppmv/decade (or 4%/decade), whereas over the period from 1980 to 2016, a positive trend of 0.06 ppmv/decade (or 2%/decade) is calculated. The interannual variation, including the drop in value around 2001, is similar to that shown by Fujiwara et al. (2010) based on balloon-borne measurements over the tropics. The seasonal variation of the water vapor reconstruction is also consistent with the MLS measurements (Figure 4b), in addition to the estimates by Fueglistaler et al. (2005) and Ploeger et al. (2011). There also appears to be broad agreement with the water vapor anomaly in the midlatitude middle stratosphere shown in Figure 4 of Hegglin et al. (2014), who merged data from multiple satellites with the help of a chemistry-climate model, if one assumes a time lag of 3.5 years (i.e., reconstruction follows by 3.5 years).

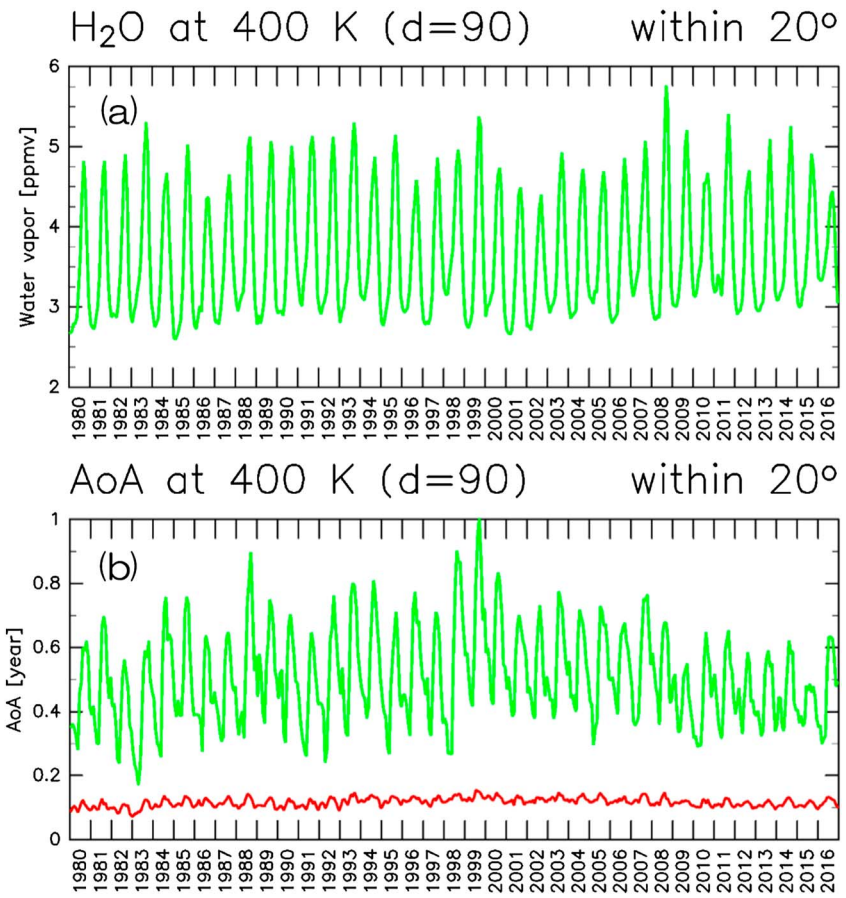

Figure 3. Time series of the (a) water vapor mixing ratio and (b) AoA reconstructed at 400-K potential temperature, averaged over 20°S–20°N (green lines). For comparison, the averaged advection time back to the troposphere Γ_T is also shown in (b; red line). AoA = age of air.

For the AoA reconstruction, the interannual and seasonal variations are shown in Figure 5 together with those for Γ_T. The seasonal variation ranges from 0.3 to 0.7 years, with a minimum in May and a maximum in August. The AoA also exhibits somewhat distinct interannual variations; in particular, the long-term variation between 1980 and 1999 is associated with a positive trend (0.08 years/decade), whereas between 1999 and 2016 a negative trend (-0.11 years/decade) occurs. These variation patterns are similar to those in $\overline{f_S}$. In contrast, the advection return time to the troposphere shows minimal seasonal or interannual variation; it is relatively constant with a value of approximately 0.1 years. This suggests that seasonal and interannual variations in Γ^{t400} are largely controlled by mixing processes between the TTL and extratropical LS. Accounting for the range of uncertainty discussed in Appendix A, the trends during 1980–1999 and 1999–2016 change from 0.03 to 0.14 years/decade and -0.04 to -0.20 years/decade, respectively.

3.3. AoA in the Midlatitude Stratosphere

The transit time from the upper TTL to midlatitude middle stratosphere has a broad spectrum, as shown in Figure 1. The AoA in the midlatitude stratosphere $\Gamma^{\mathrm{mid-st}}$ was calculated from the AoA reconstructions in the upper TTL and the spectra of the transit time. The time series of $\Gamma^{\mathrm{mid-st}}$ obtained by equation (11) is shown in Figure 6 together with the AoA estimated by Engel et al. (2009, 2017). For comparison, the mean transit time, *T*, after the tail correction by equation (10), and the modal time (i.e., the most probable transit time corresponding to the time of the spectral peak that was obtained from the 7-month smoothing filtered PDF) are also shown. Comparing the time series of $\Gamma^{\mathrm{mid-st}}$ with that of *T*, the AoA increment from *T* to $\Gamma^{\mathrm{mid-st}}$ somewhat reflects the contribution of the aging effect prior to entering the stratosphere (i.e., the contribution of those by air mass mixing processes between the TTL and extratropical LS and by transport from the troposphere to upper TTL).

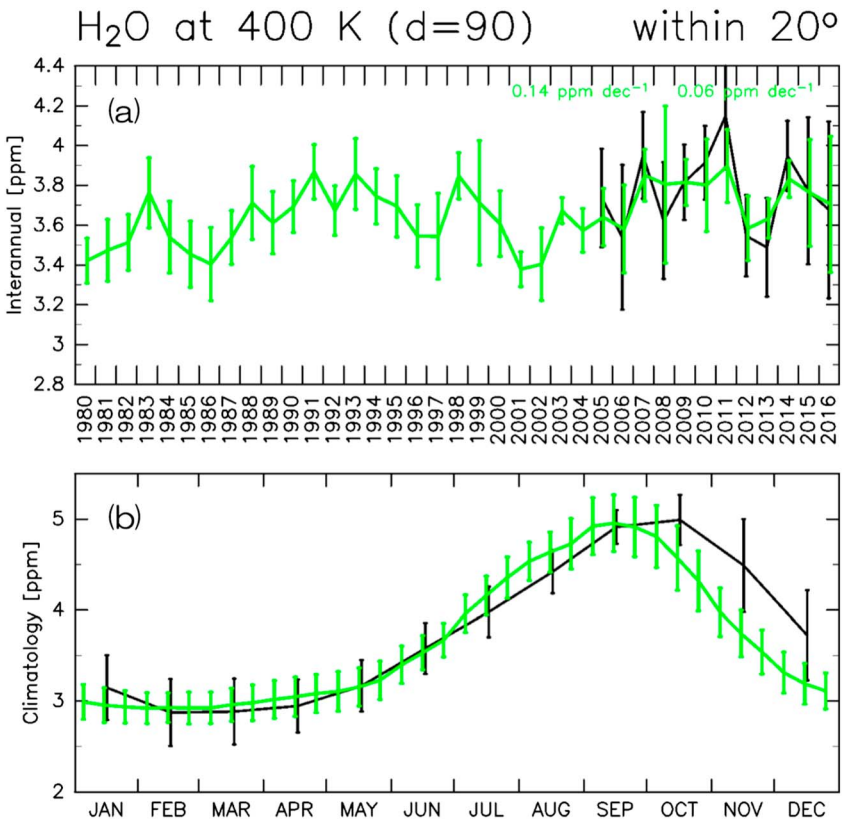

Figure 4. (a) Interannual and (b) seasonal variations in the water vapor reconstructed at 400 K over 20°S–20°N (green) which are made by deseasonalization and seasonalization of the time series shown in Figure 3a, respectively. The water vapor interannual and seasonal variations measured by MLS at 83 hPa over 20°S–20°N are also shown (black). Bars indicate one standard deviation. MLS = Microwave Limb Sounder; AoA = age of air.

The modal time, which represents the timescale of the most common path, displays an abrupt seasonal variation typically ranging from 1 to 2.5 years, where the average is approximately 1.8 years during the period 1989–2016. On the other hand, the Γ^{mid-st} has a more moderate seasonal variation which is largely forced by the seasonal variation in *T*. In turn, the seasonal variation in *T* results from the seasonal cycle in the strength of the deep branch of the BDC. The average values for T and Γ^{mid-st} are 3.1 and 3.6 years, respectively, over the period 1989–2016. Thus, the aging effect of the processes prior to entering the stratosphere is estimated as ~0.5 years on average (with contributions of ~0.4 years by in-mixing and ~0.1 years by transport from the troposphere to upper TTL, as shown in Figure 5). Accounting for the range of uncertainty discussed in Appendix A, this aging effect ranges from 0.3 to 0.8 years. The AoA Γ^{mid-st} is, however, certainly smaller than the AoA estimates by Engel et al. (2009, 2017). The reason for this difference is discussed in section 4.1. To quantify the difference between the reconstructions calculated in the present study and the estimates of Engel et al. (2009, 2017), the mean difference and root-mean-square difference between the two were calculated by adding a given increment to the reconstructions. Figure 7 shows the dependence of the statistical scores on the constant time increment which is systematically added to the modal time, *T*, and Γ^{mid-st}. A minimum in the mean difference and the root-mean-square difference is achieved with increments of ~3.1, ~1.8, and ~1.4 years for the modal time, *T*, and Γ^{mid-st}, respectively.

Similar to the trend of 0.24 years/decade in AoA for the period 1975–2005 reported by Engel et al. (2009, 2017), there are also apparent trends in the four time series shown in Figure 6. To focus on the long-term variation in these time series, trends over the period 1989–2000 are calculated. Overall, the trends in the four time series are positive with values of 0.45, 0.26, 0.22, and 0.15 years/decade for the Engel's record, Γ^{mid-st}, *T*, and the modal time, respectively. Note that for the Engel's record, 1992 and 2000 lack estimates, in addition to atypical small values in 2001. Therefore, trends for the 1989–2005 period are also calculated, resulting in 0.20, 0.19, 0.14, and 0.02 years/decade for the Engel's record, Γ^{mid-st}, *T*, and the modal time, respectively.

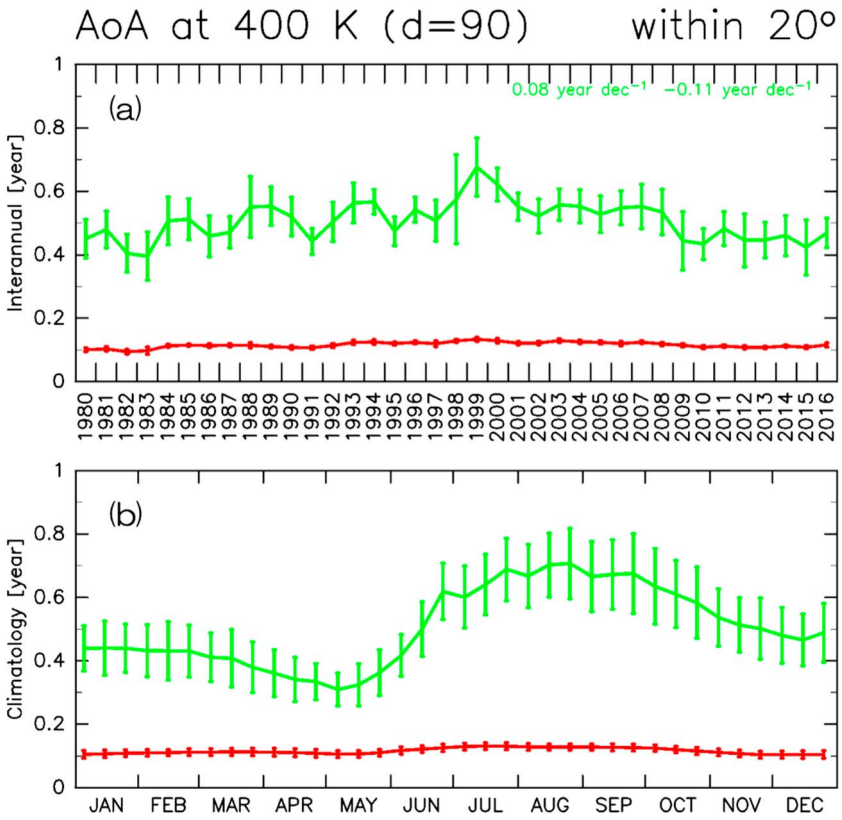

Figure 5. Same as Figure 4 but for AoA reconstructed at 400 K over 20°S–20°N (green) and the averaged advection time back to the troposphere Γ_T (red).

Toward the end of the records, although a period of missing estimates is seen in the Engel's record from 2006 to 2014, mean age estimates show a negative trend in the 2002–2016 period. For this period, the four trends are calculated to be −0.24, −0.12, −0.03, and 0.06 years/decade for the Engel's record, $\Gamma^{\mathrm{mid-st}}$, T, and the modal time, respectively. The implications of these trends are discussed in section 4.2.

4. Discussion

4.1. Possible Bias in Estimates of the Reconstructed AoA and Aging Effects

This study reconstructed AoA in the upper TTL and contiguous time series of AoA in the midlatitude middle stratosphere for comparison with the observational record of Engel et al. (2009, 2017). As described in

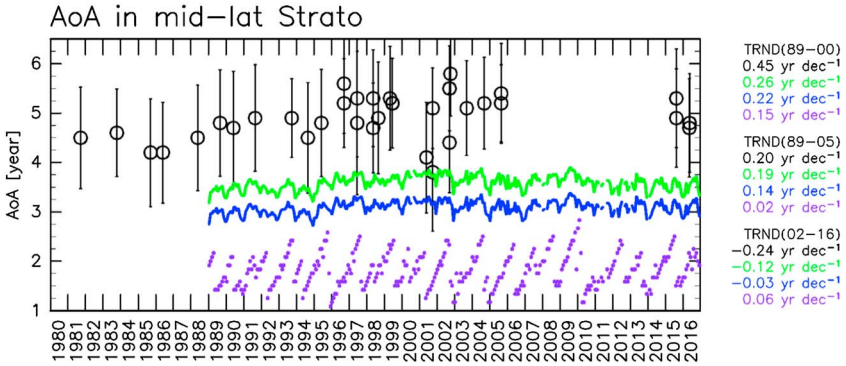

Figure 6. Time series of estimated AoA in the midlatitude middle stratosphere in the altitude/latitude region of 30–5 hPa/30°N–50°N (green). The mean transit time (blue) and modal time (purple) from the midlatitude stratosphere back to the 400 K over 20°S–20°N are also shown for comparison. The AoA estimates based on balloon measurements in the same region by Engel et al. (2009, 2017) are also shown (black circles). The vertical bars for the Engel et al. (2009, 2017) data show the measurement uncertainty estimated in their study. AoA = age of air.

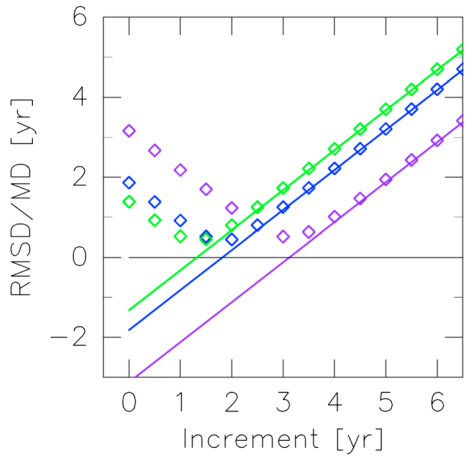

Figure 7. Relationships of the mean difference (lines) and RMS difference (diamond symbols) between the reconstructed and observed (Engel et al., 2009, 2017) AoA time series. The reconstructions for the modal time, transit time in the stratosphere, and AoA are shown in purple, blue, and green, respectively. RMS = root-mean-square; AoA = age of air.

section 3 and as seen in Figure 7, there is an evident difference between the reconstructed estimate and the observational record of approximately 1.4 years. Here we discuss possible causes for this difference. From past studies, it can be presumed that underestimations in the reconstructed estimates are due to (1) lack of aging by subgrid-scale mixing in the stratosphere and (2) young bias of AoA estimates caused by the use of kinematic trajectories.

Garny et al. (2014) investigated aging by mixing: the mixing between the tropics and extratropics in the stratosphere causes air to recirculate along the residual circulation, thereby enhancing AoA above the level at which mixing occurs. The estimation for the transit time spectrum in the current study partially considers this process with those recirculating trajectories; however, in principle the method does not have the capability to include subgrid-scale mixing processes. Second, in relation to possible bias due to the use of kinematic trajectories, the sensitivity of AoA estimation to the use of kinematic or diabatic trajectories was discussed by Schoeberl et al. (2003). It was suggested that the trajectory estimated AoA is somewhat dependent on the vertical transport condition used; therefore, the use of kinematic trajectories results in younger AoA estimates by about 1 year or more than that from diabatic trajectories. Recently, using a modern era data set (Diallo et al., 2012), the differences between the AoA estimates from using kinematic and diabatic trajectories were examined in detail when both were driven by ERA-Interim. It was suggested that in the NH stratosphere, at least in the period 2006–2009, using kinematic trajectories led to an AoA about 0.5–0.8 years younger than that using diabatic trajectories. In addition, Monge-Sanz et al. (2012) showed that the use of 6-hourly meteorological data also led to an underestimation of AoA (approximately 0.2–0.3 years younger at 20 km in the midlatitudes) in comparison to using 3-hourly data.

Overall, uncertainty still remains in quantifying the underestimation of AoA, including the AoA estimated here. However, assuming a range from 0 to 1.1 years in the underestimation and considering the contributions suggested above, the effect of aging by subgrid-scale mixing, which is simply estimated as a residual of the Engel et al. (2009, 2017) value, is thought to range from 0.0 to 1.6 years. Given this, the breakdown of aging effects to reach to midlatitude middle stratosphere is estimated to be 3.1–4.2 years (or 62–84%) by transit time in the stratosphere, 0.2–0.7 years (or 3–14%) by in-mixing prior to entering the stratosphere, 0.1 years (or 2%) by transit time from the troposphere to upper TTL and 0.0–1.6 years (or 0–32%) by subgrid-scale mixing in the stratosphere (Table 3).

4.2. The Impact of Long-Term Variation in the Mixing Fraction

This study quantified the contribution of the mixing processes between the TTL and extratropical LS that occur before air masses enter the stratosphere to long-term variation in stratospheric AoA. This was conducted using an estimation of the mixing fraction of tropospheric and stratospheric air masses in the upper TTL obtained from trajectory analysis. A key aim of the study was also to examine how much the long-term variation in mixing processes between the TTL and extratropical LS influenced AoA variation in the record of Engel et al. (2009, 2017).

Table 3
The Aging Effect Estimated for Each Process Until Reaching the Midlatitude Middle Stratosphere

Process	Contribution (year)	Percentage for Engel's estimate
Transit time from upper TTL to midlatitude stratosphere	3.1–4.2	62–84
Aging by in-mixing prior to entering the stratosphere	0.2–0.7	3–14
Transit time from troposphere to upper TTL	0.1	2
Aging by subgrid-scale mixing	1.6–0.0	32–0
Engel's AoA	5.0	100

Note. TTL = tropical tropopause layer; AoA = age of air.

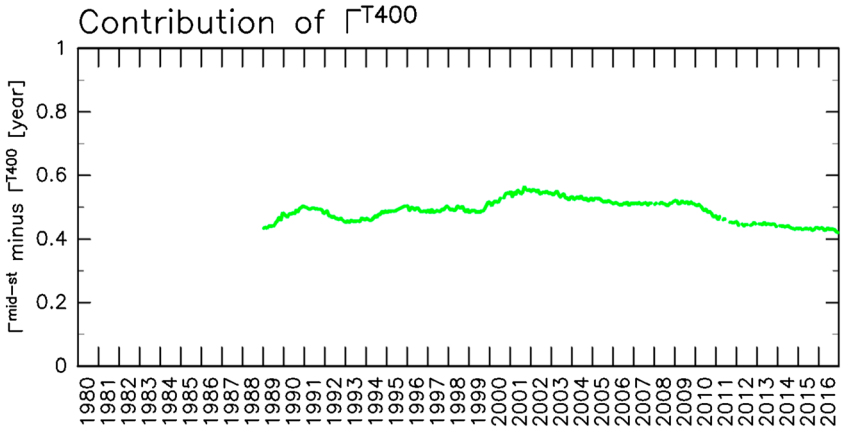

Figure 8. The contribution of Γ^{t400} to the AoA in the midlatitude stratosphere, estimated as Γ^{mid-st} minus *T*. AoA = age of air.

The stratospheric mixing fraction at the tropical 400 K surface exhibits a positive trend of 3.7%/decade for 1980–1999 and a negative trend of −5.9%/decade for 1999–2016. Subsequently, a positive trend of 0.08 years/decade for 1980–1999 and a negative trend of −0.11 years/decade for 1999–2016 are seen in the AoA time series reconstructed in the upper TTL. The upper TTL air mass is transported to the midlatitude middle stratosphere where the AoA was estimated by Engel et al. (2009, 2017). Given that the transit time has a spectral distribution as depicted in Figure 1; the impact of the variation in the upper TTL on midlatitude middle stratosphere is considered to be somewhat damped. Figure 8 shows the contribution of AoA variation in the upper TTL to that in the midlatitude stratosphere, which is estimated as Γ^{mid-st} minus *T*. The peak in 1999 in the AoA time series shown in Figure 5a is damped but eventuates as a maximum by approximately 2001 in Figure 8. Thus, the time series have a weak positive trend for 1989–2001 and a weak negative trend for 2001–2016. Even with this moderate long-term variation, there still exists good agreement between the trends from the estimates of this study and the observational record of Engel et al. (2009, 2017). For example, the trends in *T* are estimated to be 0.22, 0.14, and − 0.03 years/decade for the 1989–2000, 1989–2005, and 2002–2016 periods, respectively, and the trends in Γ^{mid-st} become 0.26, 0.19, and −0.12 years/decade for the 1989–2000, 1989–2005, and 2002–2016 periods, respectively. Therefore, the trends in Γ^{mid-st} show better agreement to those in Engel's record, estimated to be 0.45, 0.20, and −0.24 years/decade for the 1989–2000, 1989–2005, and 2002–2016 periods, respectively, than those in *T*. Overall, the long-term variation of AoA in the tropical upper TTL, which results from long-term variation in the mixing fraction, accounts for 20–80% of the difference between trends in the transit time in the stratosphere only and those in the observed AoA. The results suggest that long-term variations in the mixing process between the TTL and extratropical LS affect AoA in the upper TTL, and at least in the NH midlatitudes, the impact propagates through the deeper stratosphere.

4.3. Possible Mechanisms Driving the Variation in the Mixing Fraction

The mixing fraction of tropospheric and stratospheric air masses to estimate the AoA, as well as the water vapor mixing ratio in the upper TTL, was evaluated in this study. Here an attempt to identify the mechanisms responsible for the interannual variation seen in the mixing fraction is conducted. To this end, a time lag correlation analysis was conducted, based on monthly averaged data.

Figure 9a shows spatial distributions of the correlation coefficients between the 5-year high-pass-filtered time series of deseasonalized f_S and 2-m temperature from ERA-Interim, with a time lag of 1 month (i.e., delaying the filtered mixing fraction). It is evident that a maximum in the negative correlation coefficients occurs around the equatorial eastern Pacific so-called El Niño region. This suggests some possibility that relatively short-term variation in the mixing fraction is related to El Niño–Southern Oscillation (ENSO) activity. For example, a negative phase of the ENSO leads to enhancement of in-mixing air mass from the extratropical LS to TTL. Conversely, the supply of tropospheric air mass to the upper TTL is enhanced by a positive ENSO phase. This interpretation is in agreement with previous studies that found a strengthening of the Hadley circulation during positive ENSO events (e.g., Lu et al., 2008; Oort & Yienger, 1996).

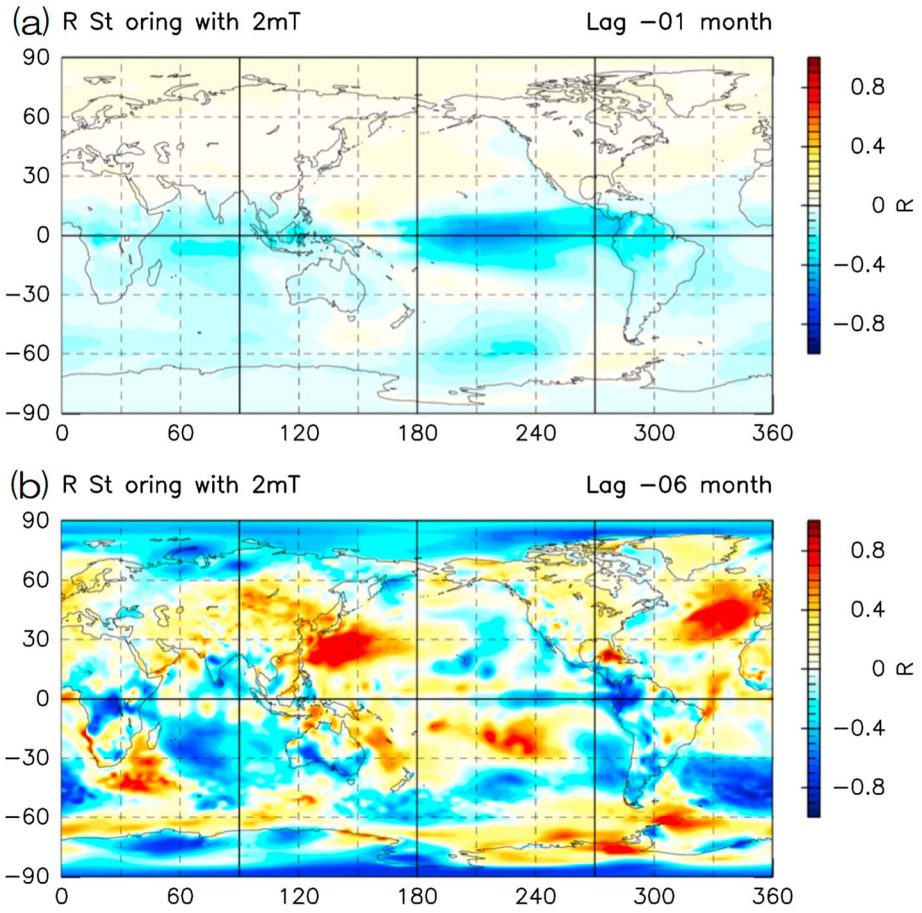

Figure 9. (a) The spatial distribution of correlation coefficients between 5-year high-pass-filtered time series of deseasonalized f_S and monthly 2-m temperature after applying the same filter with a time lag of 1 month. (b) Same as (a) but for 5-year low-pass-filtered time series with a time lag of 6 months.

Similar to Figure 9a, Figure 9b shows spatial distributions of correlation coefficients, except for the 5-year low-pass-filtered time series with a time lag of 6 months (i.e., delaying the filtered mixing fraction). The maxima of positive correlation coefficients are found over the northern Pacific and northern Atlantic oceans, where the Kuroshio and the North Atlantic Currents, respectively, exist. Further, the maxima of negative correlation coefficients are found in numerous regions, such as equatorial Africa, South America, southern Atlantic and Indian Oceans, the Arctic Sea, and Antarctica. This suggests that the long-term variation of surface air temperature (or equivalently surface temperature or the surface heat flux) in these regions affects mixing processes between the extratropical LS and TTL. Therefore, further investigation is needed to ascertain the cause(s) of the long-term change in the mixing and transport processes in the tropical and extratropical UT/LS.

4.4. Limitations of the Current Study

The interpretations described in the preceding discussion sections imply that it is necessary to consider not only the dynamical processes in the stratosphere but also those prior to entering the stratosphere to solve the puzzle of long-term variation in the stratospheric AoA. Here these were somewhat supported from an analysis taking into account the transport and grid-scale mixing process in the stratosphere. For example, some inferences were made into what processes contribute, and by how much, to the stratospheric aging and the long-term variation in AoA. However, further detailed analysis will provide increased confidence on changes in the stratospheric AoA. Further limitations of the current study not yet mentioned are described below.

One limitation of this analysis is that the mixing fraction estimated from the trajectory calculation is affected by the input meteorological data set. That said, the ERA-Interim is widely used in trajectory analysis (e.g., Hasebe & Noguchi, 2016; Konopka et al., 2015; Škerlak et al., 2014; Wang et al., 2014) and in chemistry transport/climate models (e.g., Akiyoshi et al., 2016; Dhomse et al., 2014, 2015). In particular, the ERA-Interim horizontal wind field for the UT/LS is regarded to be more accurate than that in the Modern-Era Retrospective analysis for Research and Applications (MERRA) and MERRA-2 (Jiang et al., 2015). In relation to the above, a higher-resolution ERA-Interim data set (i.e., 0.75° × 0.75° horizontal resolution, 60 vertical levels) is available. However, the lower resolution data set was used here due to computer resource limitations. To address this, additional sensitivity tests using the higher-resolution data set were conducted and confirmed that the interannual variation in the mixing fraction was not qualitatively dependent on resolution (see Appendix A).

A second limitation is that the mixing fraction is affected by the definitions of trj_T and trj_S; here each trajectory was classified as either trj_T or trj_S depending on which criterion (cri_T or cri_S) was satisfied first. However, there is the possibility that a proportion of the "tropospheric" air mass came from the region defined as "cri_S", particularly that associated with summer monsoons, which transports both tropospheric and stratospheric air masses to the tropical UT/LS. Estimates presented here, however, are consistent with the results of Homan et al. (2010) and Sargent et al. (2014), which were based on aircraft measurements. In addition to potential errors in the mixing fraction itself, the procedures used to reconstruct water vapor and AoA will introduce error into the estimates. Though the water vapor mixing ratio and AoA in the extratropical LS have interannual variation, they were treated as only seasonally varying parameters in this study. Despite this simplification, the water vapor reconstruction, especially the interannual variation, shows good agreement with the MLS measurements in the upper TTL, as well as the balloon-based measurements in the tropics shown in Figure 11 of Fujiwara et al. (2010).

5. Summary

To interpret differences between stratospheric AoA trends in the NH obtained from numerical models and observations, recent studies focused on the residual circulation and mixing processes in the stratosphere (Dietmüller et al., 2017; Garny et al., 2014; Ploeger et al., 2015). Overall, it was suggested that mixing in the stratosphere plays a crucial role in determining the trend in AoA. The focus of the current study was on mixing processes between the TTL and the extratropical LS, its impact on the AoA, and its long-term variation. The mixing fraction of tropospheric and stratospheric air masses in the upper TTL was estimated using trajectory analysis following Hasebe and Noguchi (2016). The water vapor mixing ratio and AoA in the upper TTL were reconstructed following Ploeger et al. (2012). The estimated mixing fraction and water vapor variations were largely consistent with previous studies based on aircraft and satellite measurements. Sensitivity analyses indicate that although mean values of the mixing fraction were strongly dependent on the choice of the stratospheric origin criterion, the variability was robust. From time lag correlation analysis, it is implied that such interannual variation in the mixing fraction may be caused in part by ENSO activity over shorter periods and by midlatitude phenomena over longer periods.

To compare the AoA reconstruction in detail to the observational record in the midlatitude middle stratosphere of Engel et al. (2009, 2017), the transit time in the stratosphere was accounted for. For example, the spectra of transit time from the tropical 400-K surface to the midlatitude middle stratosphere were estimated for each month during the period 1989–2016 by using a trajectory technique. The long-term variation in AoA in the midlatitude stratosphere for 1989–2016 was subsequently evaluated by the integration of the AoA reconstruction in the upper TTL together with the transit time spectra. As a result, AoA in the midlatitude stratosphere on average was estimated to be 3.6 years, approximately 1.4 years different to that of Engel's record. Accounting for possible underestimations of the average transit time in the stratosphere, the aging effects of each process were estimated to be 3.1–4.2 years (or 62–84%) for transit time in the stratosphere, 0.2–0.7 years (or 3–14%) for in-mixing prior to entering the stratosphere, 0.1 years (or 2%) for transit time from troposphere to upper TTL, and 0.0–1.6 years (or 0–32%) for subgrid-scale mixing in the stratosphere.

In terms of trends, the AoA trend in the upper TTL, which is a result of long-term variation in the mixing fraction, accounted for 20–80% of the difference between trends in the transit time in the stratosphere and that in the observed AoA. This result implies that long-term variations in the mixing processes between the TTL

and extratropical LS affect AoA in the upper TTL, and at least in the NH midlatitudes, the impact propagates through the deeper stratosphere.

Appendix A: Sensitivity Analyses and Uncertainty

Certainty of the mixing fraction in the upper TTL, as estimated in the current study, may depend on several parameters. Therefore, here the associated qualitative robustness and quantitative uncertainty for estimating the mixing fraction are detailed.

A1. Resolution of ERA-Interim

Trajectory calculations are known to be affected by the resolution of the input meteorological data set. Here the coarser resolution ERA-Interim data was used due to computing resource limitations. Therefore, the sensitivity of the results to using different resolutions was tested. The sensitivity test was conducted using the trajectories launched at the tropical 400-K potential temperature surface on the 15th of each month every 5 years from 1980 to 2015. Figure A1a shows the dependency of the mixing fractions on the resolution of meteorological data. The mixing fractions calculated from ERA-Interim data used in this study (1.5° × 1.5° horizontal resolution, 37 vertical levels) are compared with those with the higher resolution (0.75° × 0.75° horizontal resolution, 60 vertical levels) and by changing the critical latitude for the determination of stratospheric origin in cri_S from 30° to 50°. The mixing fractions for each run depicted by small dots are distributed in a linear fashion, and the annual averages are distributed similarly, with slopes of ~1.5, ~1.2, and ~0.8 for critical latitudes of 30°, 40°, and 50°, respectively. This suggests that the mixing fractions are dependent on the critical latitude and that the interannual variation of the mixing fractions could potentially be ~1.5 times larger if the higher-resolution data were used with no change in cri_S. However, they are not qualitatively dependent on different resolutions of the input data.

Criteria for categorizing tropospheric and stratospheric air parcels.

The results are predicated on the trajectory calculation, as well as categorizing individual trajectories by using the criteria cri_T and cri_S, as explained in section 2.1. The configuration of such criteria affects the evaluation of the mixing fractions. Here the results of sensitivity tests for the configuration of criteria are discussed. First, somewhat different definitions than Ploeger et al. (2012) for categorizing stratospheric trajectories were used (i.e., latitude and potential vorticity in this study compared with equivalent latitude in Ploeger et al., 2012). The reason for not employing equivalent latitude was also due to computing resource limitations owing to the calculation of equivalent latitude requiring a large amount of computational effort, especially here where the analysis extended 37 years. Therefore, the mixing fractions evaluated by the two definitions are compared for selected periods. Figures A1b and A1c compare the results obtained from the definition employed in the current study and those obtained from Ploeger's definition using equivalent latitude. This comparison is conducted two ways. First, a comparison between the mixing fractions evaluated with the coarser resolution (1.5° × 1.5° horizontal resolution, 37 vertical levels) ERA-Interim used in this study and that evaluated from Ploeger's definition with the same data is provided (Figure A1b). Second, a similar comparison is provided but with the higher-resolution data (0.75° × 0.75° horizontal resolution, 60 vertical levels; Figure A1c). Both comparisons are performed with the critical equivalent latitude for the determination of stratospheric origin ranging from 30° to 50°. These annual averages for the critical equivalent latitude of 50° conforming to Ploeger et al. (2012) are distributed linearly with slopes of 0.2 and 0.4 for the resolution in this study and the higher-resolution data, respectively. The slopes steepen with decreasing critical equivalent latitude, with slopes up to 1.2 for the higher-resolution data. Linear distributions of these annual averages suggest that the interannual variation of mixing fractions can change quantitatively, but they are not qualitatively dependent on the use of either latitude or equivalent latitude for the categorization.

The next sensitivity test detailed here is that for the timescale used to classify whether air parcels are either of tropospheric or stratospheric origin. As described in section 2.1, 5 days was used as this criterion in this study. However, whether the mixing fractions are dependent on the timescale is considered here. Figure A1d shows the sensitivity of such a test (i.e., the comparison between mixing fractions obtained by the classification with 5-day timescales and those with timescales of 1, 3, and 7 days. It can be seen that points for each run are distributed in a linear fashion, and the annual averages are distributed similarly with the slope dependent on the timescale. Therefore, despite the interannual variations changing quantitatively, they are not qualitatively dependent on the timescale parameter.

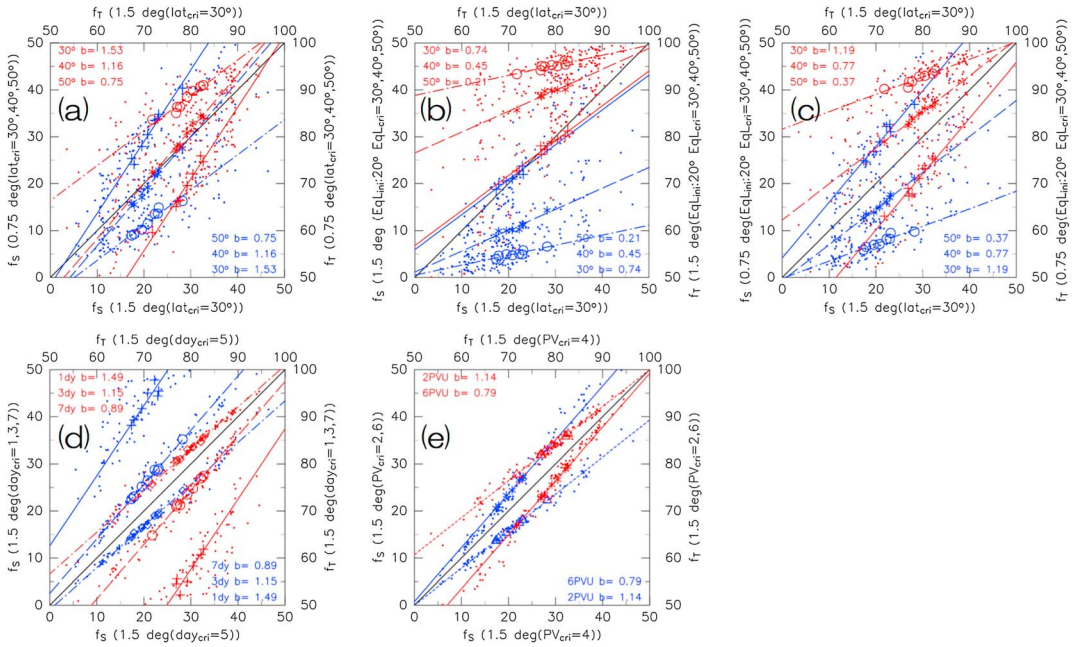

Figure A1. (a) Scatter plots of f_T (red) and f_S (blue) calculated by using ERA-Interim data with a resolution of 1.5° and 37 pressure levels versus those with 0.75° and 60 model levels. The comparison shows only values for the 15th day of each month in 1980, 1985, 1990, 1995, 2000, 2005, 2010, and 2015. Small dots indicate the mixing fractions obtained from each run of trajectory analysis. Crosses with solid lines, asterisks with dashed lines, and open circles with dash-dotted lines indicate annually averaged values and respective regression lines for 30°, 40°, 50°, respectively, applied as the critical latitude for determination of stratospheric trajectory. The numbers shown are the respective slopes of the regression lines. (b) and (c) Same as (a) but for the comparisons between the mixing fractions obtained in this study and those obtained with the use of equivalent latitude for the criteria of stratospheric origin similar to Ploeger et al. (2012) with coarser- and higher-resolution data. (d) Same as (a) but for the relationship between the time length for the determination of air mass origin in the cri_T and cri_S. Crosses with solid lines, open circles with dashed lines, and diamonds with dash-dotted lines are the annual averages and respective regression lines for the calculation using 1, 3, and 7 days applied as the time length, respectively. (e) Same as (a) but for the relationship between the potential vorticity using the cri_S. The asterisks with solid lines and triangles with dotted lines are the annual averages and respective regression lines for the calculation using 2and 6 PVU as the determination of stratospheric origin in cri_S.

Lastly, the sensitivity to the potential vorticity used to classify when air parcels are determined as stratospheric origin is tested. As described in section 2.1, 4 PVU was used in this study. However, whether the mixing fractions change with changes in this parameter from 2 to 6 PVU is examined. Figure A1e shows the dependency of mixing fractions on the potential vorticity used for classifying stratospheric origin. The points for each run are distributed in a linear fashion, and the annual averages are distributed similarly with the slope dependent on this parameter. Therefore, despite the interannual variations changing quantitatively, they are not qualitatively dependent on the value of this parameter.

A2. Uncertainty in the Mixing Fraction

The sensitivity analyses detailed above provide information to estimate the likely range of uncertainty in the mixing fraction. Assuming that the mixing fraction evaluated with the higher-resolution data is more accurate than that with the coarser resolution, the uncertainty should be derived from the comparative results shown in Figures A1a and A1c. Employing latitude in the criteria for both the launching position of trajectories and the determination for stratospheric origin, the mixing fraction f_S varies by as much as 0.8 to 1.5 times the values presented in the results with the critical latitude varying from 50° to 30° (see Figure A1a). Employing equivalent latitude in both criteria, the mixing fraction f_S varies by as much as 0.4 to 1.2 times the main result with the critical equivalent latitude varying from 50° to 30°. These results imply that the probable mixing fraction f_S falls to within 0.4 to 1.5 times the values presented in the results, whether one employs latitude or equivalent latitude in the criteria. Uncertainty arising from the critical potential vorticity in cri_S is likely included when using the critical equivalent latitude because of their physical descriptions. Indeed, the range of slopes shown in Figure A1e lies within the range in Figure A1c. Uncertainty associated with the critical timescale in cri_S and cri_T is also presumably partly included when using the critical equivalent latitude because equivalent latitude is a conservative amount; however, it is independent of uncertainty arising

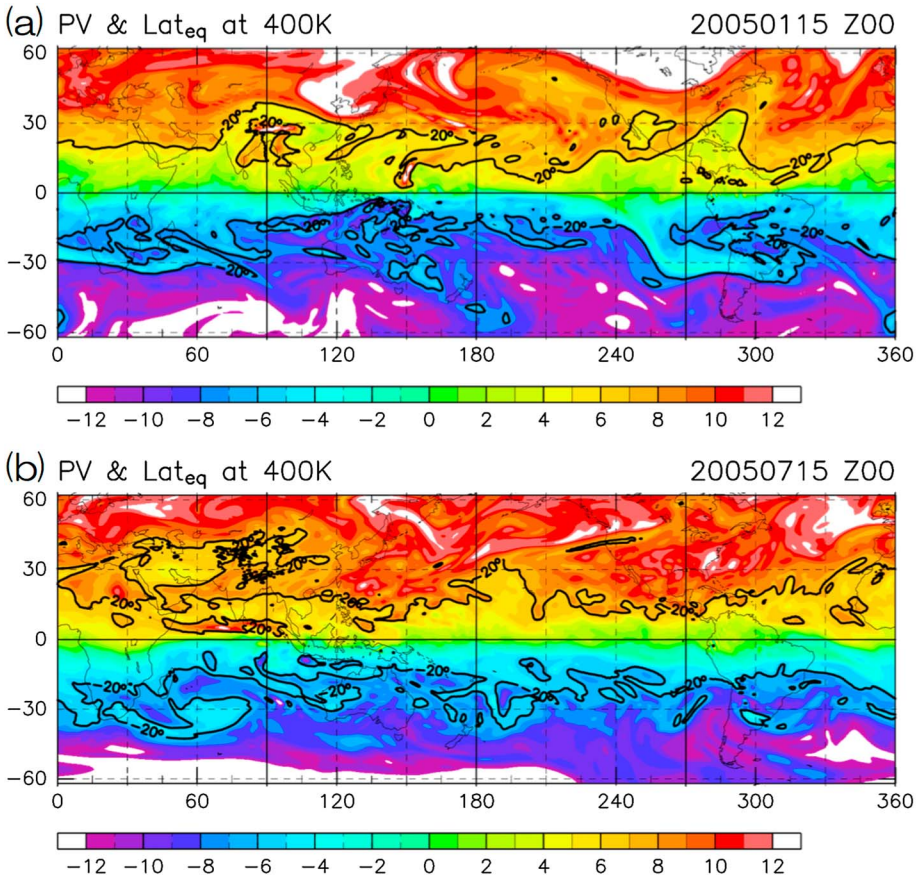

Figure B1. Horizontal distributions of potential vorticity (color in potential vorticity unit) and contours of 20°N and 20°S equivalent latitude (black lines) at the 400-K potential temperature surface for (a) 00Z on 15 January and (b) 00Z on 15 July 2005.

from the critical latitude. Results of the sensitivity analyses, in terms of the timescale, indicate that f_S can range from 0.9 to 1.2 times by varying the threshold from 7 to 3 days (see Figure A1d). Therefore, the range of the total uncertainty is estimated for the mixing fraction f_S by multiplying the range of uncertainty arising from the critical timescale only by that from critical latitude, which is equivalent to as much as 0.4 to 1.8 times the values presented in the results. Since f_S for the complete analysis period is on average ~20%, the range of uncertainty is therefore estimated to be 8–36%.

Appendix B: Quantitative Differences From Ploeger et al. (2012) and Volk et al. (1996)

The sensitivity analyses detailed in Appendix A show the strong dependency of the mixing fractions on the critical latitude or critical equivalent latitude for the determination of stratospheric origin. Overall, the range of uncertainty for estimating the mixing fraction in the current study is consistent with that in Ploeger et al. (2012); their estimate approximately fits within the lower limit of the range. Their conservative estimate is also in good agreement with that of Volk et al. (1996). In this section, we discuss how differences in the criteria result in different mixing fraction estimates and consider the factors that determine the quantitative differences in the mixing fraction estimates.

The mixing fraction of Ploeger et al. (2012) was estimated by using back trajectories originating at 400 K and 20°S–20°N equivalent latitude. However, as shown in Appendix A, the results are highly sensitive to the critical equivalent latitude for the determination of stratospheric origin, while at the same time the use of equivalent latitude produces a smaller mixing fraction f_S than that with the use of latitude (compare Figure A1a with A1c). Here we discuss how the use of equivalent latitude leads to smaller estimates of f_S. Figure B1 shows the horizontal distributions of the potential vorticity and 20°S and 20°N equivalent latitudes at 400 K for 00Z

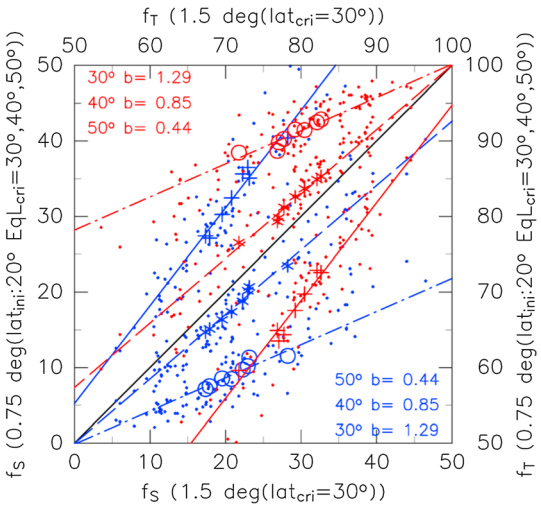

Figure B2. Same as Figure A1c but for the results when initial latitude is used instead of equivalent latitude for the selection of back trajectories in the method of Ploeger et al. (2012). Comparison was made with the critical equivalent latitude setting in the Ploeger's criteria for stratospheric origin as 30°, 40°, 50°.

on 15 January and July 2005 obtained from ERA-Interim. It is apparent that several air masses, whose equivalent latitude is higher than 20°S or 20°N, have migrated close to the equator as it is called in-mixing. Such areas were not included in the estimation using equivalent latitude as the criterion of initial positions, whereas uniformly distributed initial positions within 20°S–20°N latitude were used in this study to estimate the mixing fraction. It is perceived that this difference is one reason why the estimate of f_S reduces when evaluated with their initial position based on equivalent latitude. It is uncertain whether the suction up by the BDC acts on the tropical air mass at 400 K uniformly or not. However, it should not preferentially act only on air masses whose equivalent latitude is lower than 20°S and 20°N. Therefore, the approach used in this study is deemed most appropriate for the purpose of comparing with AoA in the deeper stratosphere. In that sense, the comparison between that estimated in this study and that by the same stratospheric criteria of Ploeger et al. (2012) except using initial latitudes within 20°S–20°N, instead of equivalent latitude, is shown in Figure B2 with the critical equivalent latitude changing from 30° to 50°. The differences between the two estimates reduce less than that shown in Figure A1c. The results

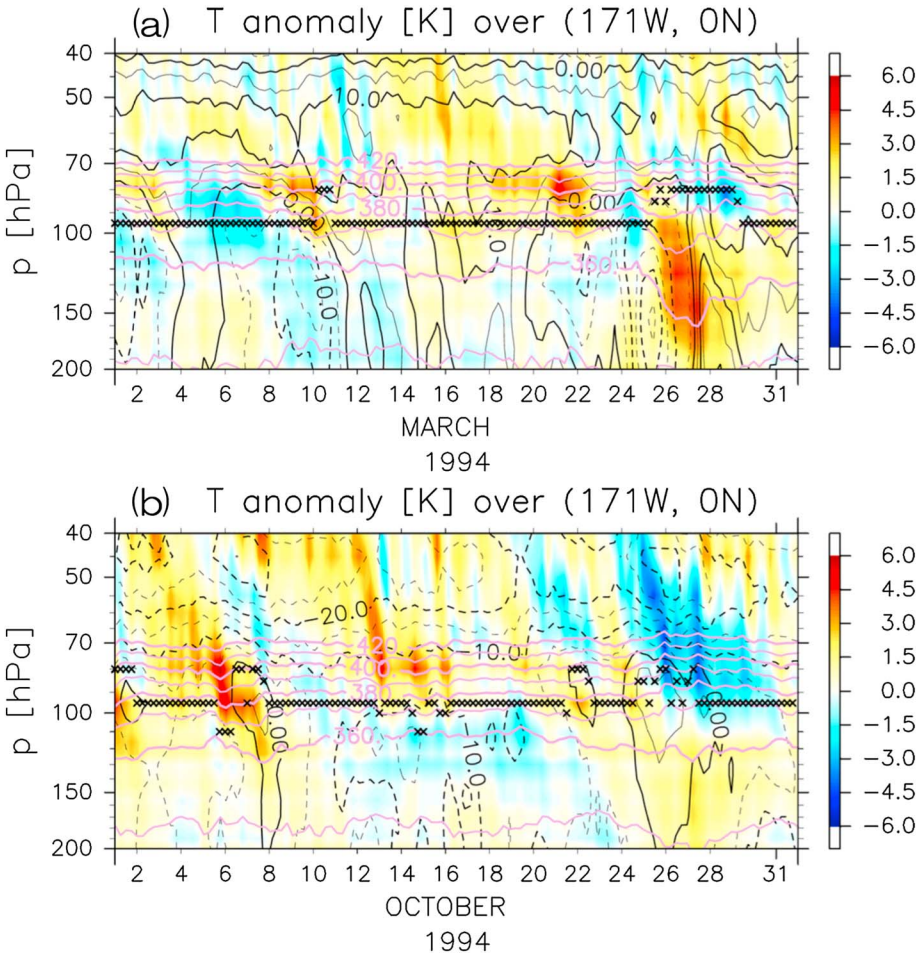

Figure B3. The time-pressure cross section of temperature anomalies (color in kelvin), zonal wind (black lines), and potential temperature (purple lines) over the equator at 171°W in (a) March and (b) October 1994. The black x symbols indicate the cold point tropopause.

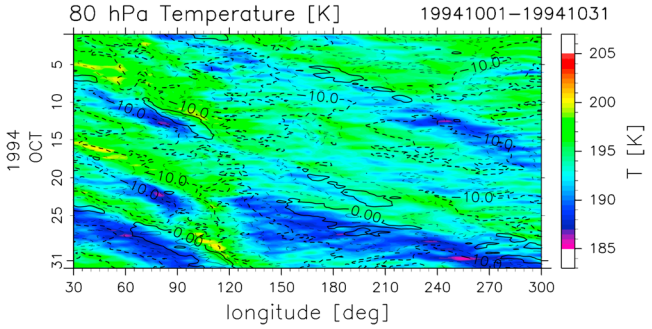

Figure B4. The longitude-time cross section of the equatorial temperature (color) and zonal wind (contour) at 80 hPa in October 1994.

are highly sensitive to critical equivalent latitude; however, it was confirmed whereby the critical equivalent latitude was set to 37°, resulting in the two estimates agreeing both qualitatively and quantitatively.

The mixing fraction observationally estimated by Volk et al. (1996) also approximately fits within the lower range limit of uncertainty for estimating the mixing fraction in the current study, being as conservative as that in Ploeger et al. (2012). Here possible reasons are considered. Aircraft campaign (the Airborne Southern Hemisphere Ozone Experiment/Measurements for Assessing the Effects of Stratospheric Aircraft: ASHOE/MAESA) data, which was used to estimate the mixing fraction of midlatitude air in Volk et al. (1996), are described in Tuck et al. (1997). According to Tuck et al. (1997), the measurements in the equatorial region were conducted on 21 and 22 March and on 24, 26, and 29 October 1994; periods that correspond to seasons when the mixing fraction in the present study and in Ploeger et al. (2012) are at a minimum. In addition, Tuck et al. (1997) presented vertical profiles of N_2O, CO_2, and CFC-11 during the two periods in their Figures 12–14. The N_2O profile in the equatorial region was shown to decrease with increasing height above ~365 K potential temperature in late March but remained constantly low up to 405-K potential temperature in late October. The vertical profiles of CFC-11 were also shown to exhibit large differences between late March and late October. The mixing fraction estimated by Volk et al. (1996) is based on these profiles that have large differences depending on the measurement periods.

The ERA-Interim data are useful for understanding what process caused the large differences in vertical profiles between the two periods during the aircraft campaign. Figure B3 shows the time-height cross section of the meteorological fields midway (i.e., 171°W, 0°N) between Hawaii and Fiji, where the ASHOE/MAESA campaign was conducted. While there is a warm anomaly in the upper TTL (note that a concept of TTL was not common at that time) around 21 March, the TTL structure was not disturbed during the observational period. Conversely, a strong cold anomaly propagating from above uplifts the potential temperature surfaces in the upper TTL as well as the cold point tropopause up to the 390-K potential temperature level around 26 October. The Hovmöller diagram (Figure B4) shows that the strong cold anomaly propagated eastward from the Indonesian region. The propagation speed corresponds to typical speeds for the equatorial Kelvin wave (e.g., Suzuki et al., 2010); thus, the propagating cold anomaly appears to be the uplifting phase of an equatorial Kelvin wave (e.g., Fujiwara et al., 1998). Therefore, a tropospheric air mass was fortuitously lifted higher than usual by the atmospheric wave during which the equatorial UT/LS was observed by the ASHOE/MAESA campaign in late October 1994. This would lead to such a condition where the mixing fraction of the tropospheric air mass was temporally enhanced or that of the stratospheric air mass was reduced.

Acknowledgments

This work was supported by Grants-in-Aid for Scientific Research (15 K17760 and 26220101) from the Japanese Society for the Promotion of Science and the Arctic Challenge for Sustainability (ArCS) Project by the Ministry of Education, Culture, Sports, Science and Technology, Japan. The author thanks Fumio Hasebe and Satoshi Sugawara for helpful discussions. Engel's AoA data were downloaded from supporting information of Engel et al. (2009; URL: https://images.nature.com/full/nature-assets/ngeo/journal/v2/n1/extref/ngeo388-s1.pdf) for 1975−2005 and are referred to in the text as Engel et al. (2017) for 2015 and 2016. Appreciation is given to ECMWF for providing the ERA-Interim data and to the NASA Jet Propulsion Laboratory for providing the Aura/MLS data. All figures were produced with the GFD-DENNOU Library. The author is also grateful to the Editor William Randel and sincerely appreciates three reviewers who provided constructive comments that greatly improved the manuscript.

References

Akiyoshi, H., Nakamura, T., Miyasaka, T., Shiotani, M., & Suzuki, M. (2016). A nudged chemistry-climate model simulation of chemical constituent distribution at northern high-latitude stratosphere observed by SMILES and MLS during the 2009/2010 stratospheric sudden warming. *Journal of Geophysical Research: Atmospheres*, *121*, 1361–1380. https://doi.org/10.1002/2015JD023334

Bönisch, H., Engel, A., Curtius, J., Birner, T., & Hoor, P. (2009). Quantifying transport into the lowermost stratosphere using simultaneous in-situ measurements of SF6 and CO2. *Atmospheric Chemistry and Physics*, *9*(16), 5905–5919. https://doi.org/10.5194/acp-9-5905-2009

Butchart, N., Cionni, I., Eyring, V., Shepherd, T. G., Waugh, D. W., Akiyoshi, H., et al. (2010). Chemistry–climate model simulations of twenty-first century stratospheric climate and circulation changes. *Journal of Climate*, *23*(20), 5349–5374. https://doi.org/10.1175/2010JCLI3404.1

Dee, D. P., Uppala, S. M., Simmons, A. J., Berrisford, P., Poli, P., Kobayashi, S., et al. (2011). The ERA-Interim reanalysis: Configuration and performance of the data assimilation system. *Quarterly Journal of the Royal Meteorological Society*, *137*(656), 553–597. https://doi.org/10.1002/qj.828

Dhomse, S. S., Chipperfield, M. P., Feng, W., Hossaini, R., Mann, G. W., & Santee, M. L. (2015). Revisiting the hemispheric asymmetry in midlatitude ozone changes following the Mount Pinatubo eruption: A 3-D model study. *Geophysical Research Letters*, *42*, 3038–3047. https://doi.org/10.1002/2015GL063052

Dhomse, S. S., Emmerson, K. M., Mann, G. W., Bellouin, N., Carslaw, K. S., Chipperfield, M. P., et al. (2014). Aerosol microphysics simulations of the Mt. Pinatubo eruption with the UM-UKCA composition-climate model. *Atmospheric Chemistry and Physics*, *14*, 11,221–11,246.

Diallo, M., Legras, B., & Chédin, A. (2012). Age of stratospheric air in the ERA-Interim. *Atmospheric Chemistry and Physics*, *12*(24), 12,133–12,154. https://doi.org/10.5194/acp-12-12133-2012

Dietmüller, S., Garny, H., Plöger, F., Jöckel, P., & Cai, D. (2017). Effects of mixing on resolved and unresolved scales on stratospheric age of air. *Atmospheric Chemistry and Physics*, *17*(12), 7703–7719. https://doi.org/10.5194/acp-17-7703-2017

Engel, A., Bönisch, H., Ullrich, M., Sitals, R., Membrive, O., Danis, F., & Crevoisier, C. (2017). Mean age of stratospheric air derived from AirCore observations. *Atmospheric Chemistry and Physics*, *17*(11), 6825–6838. https://doi.org/10.5194/acp-17-6825-2017

Engel, A., Möbius, T., Bönisch, H., Schmidt, U., Heinz, R., Levin, I., et al. (2009). Age of stratospheric air unchanged within uncertainties over the past 30 years. *Nature Geoscience*, *2*(1), 28–31. https://doi.org/10.1038/ngeo388

Fueglistaler, S., Bonazzola, S., Haynes, P. H., & Peter, T. (2005). Stratospheric water vapor predicted from the Lagrangian temperature history of air entering the stratosphere in the tropics. *Journal of Geophysical Research*, *110*, D08107. https://doi.org/10.1029/2004JD005516

Fujiwara, M., Kita, K., & Ogawa, T. (1998). Stratosphere-troposphere exchange of ozone associated with the equatorial Kelvin wave as observed with ozonesondes and rawinsondes. *Journal of Geophysical Research*, *103*, 19,173–19,182.

Fujiwara, M., Vömel, H., Hasebe, F., Shiotani, M., Ogino, S. Y., Iwasaki, S., et al. (2010). Seasonal to decadal variations of water vapor in the tropical lower stratosphere observed with balloon-borne cryogenic frostpoint hygrometers. *Journal of Geophysical Research*, *115*, D18304. https://doi.org/10.1029/2010JD014179

Garny, H., Birner, T., Bönisch, H., & Bunzel, F. (2014). The effects of mixing on age of air. *Journal of Geophysical Research: Atmospheres*, *119*, 7015–7034. https://doi.org/10.1002/2013JD021417

Gettelman, A., Hoor, P., Pan, L. L., Randel, W. J., Hegglin, M. I., & Birner, T. (2011). The extra-tropical upper troposphere and lower stratosphere. *Reviews of Geophysics*, *49*, RG3003. https://doi.org/10.1029/2011RG000355

Haenel, F. J., Stiller, G. P., von Clarmann, T., Funke, B., Eckert, E., Glatthor, N., et al. (2015). Reassessment of MIPAS age of air trends and variability. *Atmospheric Chemistry and Physics*, *15*(22), 13,161–13,176. https://doi.org/10.5194/acp-15-13161-2015

Hall, T. M., & Plumb, R. A. (1994). Age as a diagnostic of stratospheric transport. *Journal of Geophysical Research*, *99*(D1), 1059–1070. https://doi.org/10.1029/93JD03192

Hasebe, F., & Noguchi, T. (2016). A Lagrangian description on the troposphere-to-stratosphere transport changes associated with the stratospheric water drop around the year 2000. *Atmospheric Chemistry and Physics*, *16*(7), 4235–4249. https://doi.org/10.5194/acp-16-4235-2016

Hegglin, M. I., Plummer, D. A., Shepherd, T. G., Scinocca, J. F., Anderson, J., Froidevaux, L., et al. (2014). Vertical structure of stratospheric water vapour trends derived from merged satellite data. *Nature Geoscience*, *7*(10), 768–776. https://doi.org/10.1038/ngeo2236

Homan, C. D., Volk, C. M., Kuhn, A. C., Werner, A., Baehr, J., Viciani, S., et al. (2010). Tracer measurements in the tropical tropopause layer during the AMMA/SCOUT-O3 aircraft campaign. *Atmospheric Chemistry and Physics*, *10*(8), 3615–3627. https://doi.org/10.5194/acp-10-3615-2010

Jiang, J. H., Su, H., Zhai, C., Wu, L., Minschwaner, K., Molod, A. M., & Tompkins, A. M. (2015). An assessment of upper troposphere and lower stratosphere water vapor in MERRA, MERRA2, and ECMWF reanalyses using Aura MLS observations. *Journal of Geophysical Research: Atmospheres*, *120*, 11,468–11,485. https://doi.org/10.1002/2015JD023752

Kida, H. (1983). General circulation of air parcels and transport characteristics derived from a hemispheric GCM, part 2, very long-term motions of air parcels in the troposphere and stratosphere. *Journal of the Meteorological Society of Japan*, *61*(4), 510–523. https://doi.org/10.2151/jmsj1965.61.4_510

Konopka, P., Grooß, J.-U., Günther, G., Ploeger, F., Pommrich, R., Müller, R., & Livesey, N. (2010). Annual cycle of ozone at and above the tropical tropopause: Observations versus simulations with the Chemical Lagrangian Model of the Stratosphere (CLaMS). *Atmospheric Chemistry and Physics*, *10*(1), 121–132. https://doi.org/10.5194/acp-10-121-2010

Konopka, P., Ploeger, F., Tao, M., Birner, T., & Riese, M. (2015). Hemispheric asymmetries and seasonality of mean age of air in the lower stratosphere: Deep versus shallow branch of the Brewer-Dobson circulation. *Journal of Geophysical Research: Atmospheres*, *120*, 2053–2066. https://doi.org/10.1002/2014JD022429

Krämer, M., Schiller, C., Afchine, A., Bauer, R., Gensch, I., Mangold, A., et al. (2009). Ice supersaturations and cirrus cloud crystal numbers. *Atmospheric Chemistry and Physics*, *9*(11), 3505–3522. https://doi.org/10.5194/acp-9-3505-2009

Li, F., Waugh, D. W., Douglass, A. R., Newman, P. A., Strahan, S. E., Ma, J., et al. (2012). Long-term changes in stratospheric age spectra in the 21st century in the Goddard Earth Observing System Chemistry-Climate Model (GEOSCCM). *Journal of Geophysical Research*, *117*, D20119. https://doi.org/10.1029/2012JD017905

Lu, J., Chen, G., & Frierson, D. M. W. (2008). Response of the zonal mean atmospheric circulation to El Niño versus global warming. *Journal of Climate*, *21*(22), 5835–5851. https://doi.org/10.1175/2008JCLI2200.1

Manney, G. L., Hegglin, M. I., Daffer, W. H., Santee, M. L., Ray, E. A., Pawson, S., et al. (2011). Jet characterization in the upper troposphere/lower stratosphere (UTLS): Applications to climatology and transport studies. *Atmospheric Chemistry and Physics*, *11*(12), 6115–6137. https://doi.org/10.5194/acp-11-6115-2011

Monge-Sanz, B. M., Chipperfield, M. P., Dee, D. P., Simmons, A. J., & Uppala, S. M. (2012). Improvements in the stratospheric transport achieved by a CTM with ECMWF (re)analyses: Identifying effects and remaining challenges. *Quarterly Journal of the Royal Meteorological Society*, *139*(672), 654–673. https://doi.org/10.1002/qj.1996

Oort, A. H., & Yienger, J. J. (1996). Observed interannual variability in the Hadley circulation and its connection to ENSO. *Journal of Climate*, *9*(11), 2751–2767. https://doi.org/10.1175/1520-0442(1996)009<2751:OIVITH>2.0.CO;2

Orbe, C., Waugh, D. W., & Newman, P. A. (2015). Air-mass origin in the tropical lower stratosphere: The influence of Asian boundary layer air. *Geophysical Research Letters*, *42*, 4240–4248. https://doi.org/10.1002/2015GL063937

Pan, L. L., Honomichl, S. B., Kinnison, D. E., Abalos, M., Randel, W. J., Bergman, J. W., & Bian, J. (2016). Transport of chemical tracers from the boundary layer to stratosphere associated with the dynamics of the Asian summer monsoon. *Journal of Geophysical Research: Atmospheres*, *121*, 14,159–14,174. https://doi.org/10.1002/2016JD025616

Ploeger, F., Abalos, M., Birner, T., Konopka, P., Legras, B., Müller, R., & Riese, M. (2015). Quantifying the effects of mixing and residual circulation on trends of stratospheric mean age of air. *Geophysical Research Letters*, *42*, 2047–2054. https://doi.org/10.1002/2014GL062927

Ploeger, F., & Birner, T. (2016). Seasonal and inter-annual variability of lower stratospheric age of air spectra. *Atmospheric Chemistry and Physics*, *16*(15), 10195–10213. https://doi.org/10.5194/acp-16-10195-2016

Ploeger, F., Fueglistaler, S., Grooß, J. U., Günther, G., Konopka, P., Liu, Y. S., et al. (2011). Insight from ozone and water vapor on transport in the tropical tropopause layer (TTL). *Atmospheric Chemistry and Physics*, *11*(1), 407–419. https://doi.org/10.5194/acp-11-407-2011

Ploeger, F., Gunther, G., Konopka, P., Fueglistaler, S., Muller, R., Hoppe, C., et al. (2013). Horizontal water vapor transport in the lower stratosphere from subtropics to high latitudes during boreal summer. *Journal of Geophysical Research: Atmospheres*, *118*, 8111–8127. https://doi.org/10.1002/jgrd.50636

Ploeger, F., Konopka, P., Müller, R., Fueglistaler, S., Schmidt, T., Manners, J. C., et al. (2012). Horizontal transport affecting trace gas seasonality in the tropical tropopause layer (TTL). *Journal of Geophysical Research*, *117*, D09303. https://doi.org/10.1029/2011JD017267

Ploeger, F., Konopka, P., Walker, K., & Riese, M. (2017). Quantifying pollution transport from the Asian monsoon anticyclone into the lower stratosphere. *Atmospheric Chemistry and Physics*, *17*(11), 7055–7066. https://doi.org/10.5194/acp-17-7055-2017

Randel, W., & Jensen, E. (2013). Physical processes in the tropical tropopause layer and their roles in a changing climate. *Nature Geoscience*, *6*(3), 169–176. https://doi.org/10.1038/ngeo1733

Santee, M. L., Manney, G. L., Livesey, N. J., Schwartz, M. J., Neu, J. L., & Read, W. G. (2017). A comprehensive overview of the climatological composition of the Asian summer monsoon anticyclone based on 10 years of Aura Microwave Limb Sounder measurements. *Journal of Geophysical Research: Atmospheres*, *122*, 5491–5514. https://doi.org/10.1002/2016JD026408

Sargent, M. R., Smith, J. B., Sayres, D. S., & Anderson, J. G. (2014). The roles of deep convection and extra-tropical mixing in the tropical tropopause layer: An in situ measurement perspective. *Journal of Geophysical Research: Atmospheres*, *119*, 12,355–12,371. https://doi.org/10.1002/2014JD022157

Schoeberl, M. R., Douglass, A. R., Zhu, Z., & Pawson, S. (2003). A comparison of the lower stratospheric age spectra derived from a general circulation model and two data assimilation systems. *Journal of Geophysical Research*, *108*(D3), 4113. https://doi.org/10.1029/2002JD002652

Škerlak, B., Sprenger, M., & Wernli, H. (2014). A global climatology of stratosphere-troposphere exchange using the ERA-Interim data set from 1979 to 2011. *Atmospheric Chemistry and Physics*, *14*(2), 913–937. https://doi.org/10.5194/acp-14-913-2014

Suzuki, J., Shiotani, M., & Nishi, N. (2010). Lifetime and longitudinal variability of equatorial Kelvin waves around the tropical tropopause region. *Journal of Geophysical Research*, *115*, D03103. https://doi.org/10.1029/2009JD012261

Tuck, A. F., Baumgardner, D., Chan, K. R., Dye, J. E., Elkins, J. W., Hovde, S. J., et al. (1997). The Brewer-Dobson circulation in the light of high-altitude in situ aircraft observations. *Quarterly Journal of the Royal Meteorological Society*, *123*, 1–69.

Vogel, B., Günther, G., Müller, R., Grooß, J.-U., Afchine, A., Bozem, H., et al. (2016). Long-range transport pathways of tropospheric source gases originating in Asia into the northern lower stratosphere during the Asian monsoon season 2012. *Atmospheric Chemistry and Physics*, *16*(23), 15,301–15,325. https://doi.org/10.5194/acp-16-15301-2016

Volk, C. M., Elkins, J. W., Fahey, D. W., Salawitch, R. J., Dutton, G. S., Gilligan, J. M., et al. (1996). Quantifying transport between the tropical and mid-latitude lower stratosphere. *Science*, *272*(5269), 1763–1768. https://doi.org/10.1126/science.272.5269.1763

Wang, T., Randel, W. J., Dessler, A. E., Schoeberl, M. R., & Kinnison, D. E. (2014). Trajectory model simulations of ozone (O_3) and carbon monoxide (CO) in the lower stratosphere. *Atmospheric Chemistry and Physics*, *14*(14), 7135–7147. https://doi.org/10.5194/acp-14-7135-2014

Waugh, D. W., & Hall, T. M. (2002). Age of stratospheric air: Theory, observations and models. *Reviews of Geophysics*, *40*(4), 1,010. https://doi.org/10.1029/2000RG000101

Waugh, D. W., Oman, L., Kawa, S. R., Stolarski, R. S., Pawson, S., Douglass, A. R., et al. (2009). Impact of climate change on stratospheric ozone recovery. *Geophysical Research Letters*, *36*, L03805. https://doi.org/10.1029/2008GL036223